Scientific Research Publishing

Journal of Applied Mathematics and Physics, 2025, 13(5), 1762-1779
https://www.scirp.org/journal/jamp
ISSN Online: 2327-4379
ISSN Print: 2327-4352

Sliding Mode Control of Chaotic Motion in Electrodynamic Tethered Satellite System in an Inclined Elliptical Plane

Ahmad Yousof Ahmad Taha[1*], Ahmed Magdy Abdelaziz[2], Abd El Hakeem Abd El Naby[1], Yehia A. Abdel-Aziz[2]

[1]Mathematics Department, Damietta University, Damietta, Egypt
[2]National Research Institute of Astronomy and Geophysics (NRIAG), Cairo, Egypt
Email: *A.usf@du.edu.eg

How to cite this paper: Taha, A.Y.A., Abdelaziz, A.M., Abd El Naby, A.E.H. and Abdel-Aziz, Y.A. (2025) Sliding Mode Control of Chaotic Motion in Electrodynamic Tethered Satellite System in an Inclined Elliptical Plane. *Journal of Applied Mathematics and Physics*, **13**, 1762-1779.
https://doi.org/10.4236/jamp.2025.135098

Received: April 8, 2025
Accepted: May 23, 2025
Published: May 26, 2025

Abstract

This paper investigates the chaotic behavior of an electrodynamic tethered satellite system (ETSS) orbiting Earth in an inclined elliptical orbit. The system is modelled using a dumbbell model. The presence of chaos is established through the computation of transversal heteroclinic orbits, and the corresponding parameter domain for chaotic motion is determined using the Melnikov function. A tether length control strategy based on sliding mode control is proposed to suppress the chaotic motion. Finally, numerical simulations are presented to validate the occurrence of chaos within the identified parameter domain and its control.

Keywords

Chaos, Electromagnetic Force, Melnikov Analysis, Poincaré Section, Sliding Mode Control, Tethered Satellite System

1. Introduction

A tethered satellite system (TSS) consists of a satellite connected to its host spacecraft by a strong cable or tether. Due to their vast potential for applications in space, Tethered Satellite Systems (TSSs) have attracted significant attention over the past few decades [1]-[4]. One of these applications is space debris removal [5]-[7]. Recently, the amount of debris has noticeably risen due to the growing number of satellites being launched [8] [9]. To ensure the safety of future satellite missions, it is crucial to eliminate this debris to stop its accumulation[10]-[14]. Researchers have shown significant interest in nonlinear features like bifurcation

and chaos [15]-[17]. Yu *et al.* [18] described the chaotic behavior of an in-plane TSS induced by atmospheric drag and Earth's oblateness. The presence of chaos is identified through transversal heteroclinic orbits, and the parameter domain for chaos to occur is determined using the Melnikov function. Additionally, a tether length control method based on a sliding-mode controller is proposed to suppress the chaotic motion to an assigned motion. Salazar [19] derived the attitude equations of a TSS and analyzed chaotic motion in both planar and coupled motion in a circular orbit. He proposed a tether length control scheme that extends the tether to a maximum length by varying the tension in the tether. Tong and Rimrott [20] investigated numerically using Poincaré maps and analytically using the Melnikov method the planar motion of satellites in elliptical orbits with different eccentricities and different inertia moment ratios, showing that there exist chaotic regions. Karasopoulos and Richardson [21] studied the nonlinear dynamics of the pitch equation of motion for a gravity-gradient satellite in an elliptical orbit about a central body. Bifurcation plots, Poincaré maps, and Lyapunov exponents were numerically calculated. It was found that the instability of the pitch angle for a gravity-gradient satellite generally increases with increasing values of orbit eccentricity. Fujii and Ichiki [22] analyzed the nonlinear dynamics of the TSS with a constant natural tether length by considering the complex effects of two system parameters: the orbital eccentricity of the Shuttle and the longitudinal rigidity of the tether. When either of these parameters is considered, the motion of the TSS becomes chaotic, depending on the system parameters and initial conditions. Misra *et al.* [23] derived three-dimensional motion equations for a two-body TSS and analyzed them numerically using methods such as phase portraits, spectral analysis, Poincaré sections, and Lyapunov exponents. Both planar and coupled motion in circular and elliptical orbits were studied, concluding that the size of the chaotic region increases with eccentricity. Peláez and Lara [24] introduced an algorithm based on the Poincaré method of continuation of periodic orbits for ETSS in inclined orbits, which led to unstable periodic solutions unsuitable for the operation of an electrodynamic tether. Kojima and Sugimoto [25] analyzed the stability of in-plane and out-of-plane motions of three-mass electrodynamic tether (EDT) systems in elliptical and inclined orbits. The occurrence of chaos is demonstrated using numerical simulations. It is found that delayed feedback control cannot stabilize the librational motion of an EDT in such orbits with high eccentricity.

In this paper, we investigate the chaotic behavior and its control of the TSS, which is modelled as a dumbbell in the station-keeping phase, orbiting Earth in an inclined elliptical orbit. The system is influenced by the Lorentz force resulting from the current flowing through the tether and the Earth's magnetic field. Additionally, the system is affected by the orbit's elliptical nature. The Melnikov function is used to derive the necessary conditions for chaos to occur. Tether length control based on sliding mode control is derived to control the chaotic system to either a desired trajectory or to guide the chaotic motion to a desired equilibrium point. Numerical simulations based on the Tether Physics and Survivability Ex-

periment mission were conducted to verify the occurrence of chaotic motion and to ensure the ability of the controller.

2. Mathematical Model

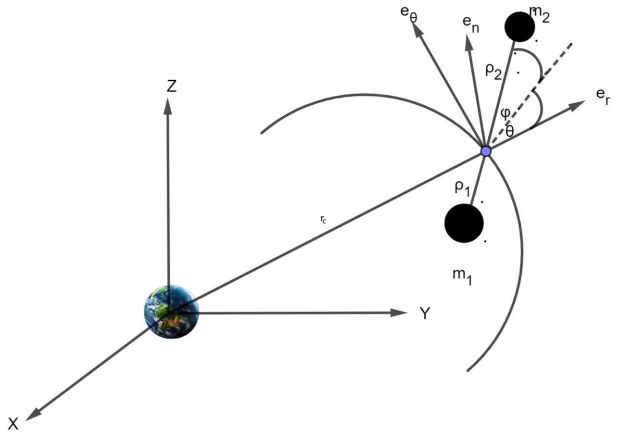

Figure 1. Tethered satellite system.

The TSS is modelled as a two-mass system, where m_1 and m_2 represent the mother satellite and subsatellite, respectively. These masses are connected by a tether of maximum length l_r with a mass of m_t. We consider an inertial frame centered at the center of the Earth (X, Y, Z), The X-axis is oriented toward the vernal equinox, the Z-axis aligns with Earth's rotation axis, and the Y-axis lies within Earth's equatorial plane, maintaining a right-handed coordinate system. Additionally, there is a rotating frame situated at a position r_c relative to the inertial frame, which is the center mass of the system (CMS). It comprises three mutually orthogonal unit vectors, where the e_θ is oriented along the velocity direction perpendicular to e_r which points radially outward, opposite to Earth's center of mass, and e_n completes the right-handed coordinate triad. The relative position vectors $\boldsymbol{\rho}_1$ and $\boldsymbol{\rho}_2$ represent the positions of the mother satellite and subsatellite, respectively, relative to the system's center of mass. The variable θ represents the in-plane angle, φ, is the out of plane angle, while l denotes the tether length at any given time. The system moves in an elliptical plane orbit around the Earth (**Figure 1**).

Libration Equations of Motion

To construct the Lagrangian of the system, we need a suitable expression for both kinetic and potential energies. To determine the total kinetic energy of a TSS with a continuous tether, we employ a combined approach: calculate the kinetic energies of the two end bodies (mother and subsatellite) and integrate the kinetic energy over the tether's length [26].

$$T = \frac{1}{2} m \dot{\boldsymbol{r}}_c \cdot \dot{\boldsymbol{r}}_c + \frac{1}{2} \mu_e \left(\dot{l}^2 + l^2 \left(\dot{\theta} + \dot{\nu} \right)^2 \right), \tag{1}$$

where $m = m_1 + m_2 + m_t$ is a total mass, $\mu_e = (m_1 + m_t/2)(m_2 + m_t/2)/(m_1 + m_2 + m_t) - m_t/6$ is a reduced mass, and ν is the true anomaly.

The potential energy of the TSS in a terrestrial gravitational field is the sum of the potential energies of the system's elements:

$$W = -\frac{\mu m_1}{r_1} - \frac{\mu m_2}{r_2} - \frac{\mu m_t}{r_C}, \tag{2}$$

where μ is Earth's gravitational strength constant. r_1 and r_2 are the radius vectors of particles m_1 and m_2. After some calculations and noticing that the tether length is at least 10 times less than the radius vector of the centre of masses, we can write the potential energy in the form

$$W = -\frac{\mu m}{r_C} - \frac{\mu \mu_e l^2}{2r_C^3}\left(3\cos^2\theta - 1\right). \tag{3}$$

With the kinetic and potential energies in Equations (1) and (3), we may now construct the Lagrangian function, $\mathcal{L} = T - W$. The Lagrange equation has the form

$$\frac{\mathrm{d}}{\mathrm{d}t}\frac{\partial \mathcal{L}}{\partial \dot{q}_i} - \frac{\partial \mathcal{L}}{\partial q_i} = Q_i, \tag{4}$$

where $q_i = \theta$, l is generalized coordinates, and Q_i is not potential generalized forces.

The equations of motion in an elliptical orbit are

$$\theta'' - \frac{2e\sin\nu}{1+e\cos\nu}\left(\theta'+1\right) + 2\left(\theta'+1\right)\frac{L'}{L} + \frac{3\cos\theta\sin\theta}{1+e\cos\nu} = \frac{Q_\theta}{\mu_e l^2 \dot{\nu}^2} \tag{5}$$

$$L'' - \frac{2e\sin\nu}{1+e\cos\nu}L' - L\left[\left(\theta'+1\right)^2 - \frac{3\cos^2\theta - 1}{1+e\cos\nu}\right] = \frac{Q_l}{\mu_e \dot{\nu}^2}, \tag{6}$$

here, the accent means a derivative with respect to variable ν, $L = l/l_r$, $\dot{\nu}^2 = \mu k^4/a^3\left(1-e^2\right)^3$, a is apogee radius, e is an eccentricity, and $k = 1 + e\cos\nu$.

The components of the non-tilted dipole model within the orbital coordinate system are denoted as B_r, B_θ and B_n, respectively, can be determined as follows [27]:

$$B_r = -2\frac{\mu_m}{r_c^3}\sin\nu\sin i, \tag{7}$$

$$B_\theta = \frac{\mu_m}{r_c^3}\cos\nu\sin i, \tag{8}$$

$$B_n = \frac{\mu_m}{r_c^3}\cos i, \tag{9}$$

where i is an orbital inclination and μ_m is the magnitude diploe of Earth = 7.85×10^{15} N/A m^2.

When an electric current traverses the conducting tether wire amidst a magnetic field, a force arises in a direction perpendicular to both the local magnetic

field lines and the direction of the current. The Lorenz force acting on the differential length element $\mathrm{d}s$ of the tether is expressed as:

$$\mathrm{d}\boldsymbol{F} = I\left(\boldsymbol{t}\times\boldsymbol{B}\right)\mathrm{d}s, \tag{10}$$

here, I denotes the current flowing through the tether, $\boldsymbol{t}$ represents the unit vector tangent to the tether line in the direction of s, and $\boldsymbol{B}$ is the geomagnetic field vector measured at the system's centre of mass. Although the tether length potentially extends over several kilometres, it is markedly small compared to the orbital radius. Consequently, it is assumed that the geomagnetic field vector remains constant along the entire length of the tether, consistent with its value at the system's centre of mass.

Following the principle of virtual work, the generalized electromagnetic torques can be determined as:

$$Q_{q_j} = \int_{-\rho_1}^{\rho_2} \mathrm{d}\boldsymbol{F}\cdot\frac{\partial \boldsymbol{R}}{\partial q_j} = \int_{-\rho_1}^{\rho_2} I\left(\boldsymbol{t}\times\boldsymbol{B}\right)\cdot\frac{\partial \boldsymbol{R}}{\partial q_j}\mathrm{d}s, \tag{11}$$

where $\boldsymbol{R}$ is the inertial vector to the line of action of the force $\mathrm{d}\boldsymbol{F}$ acting on the position of $\mathrm{d}s$. For the case of constant current value in the tether and integrating Equation (11), leads to the generalized torques Q_θ, Q_l where the out-of-plane angle equals zero in our planar motion

$$\begin{aligned} Q_\theta &= -\frac{Il^2\left(m_2-m_1\right)}{2\left(m_1+m_2+m_t\right)}B_n, \\ Q_l &= 0. \end{aligned} \tag{12}$$

Substituting Equation (12) into Equations (5)-(6) with $r_c = a\left(1-e^2\right)/k$, we can write the equations of motion of the system

$$\theta'' - \frac{2e\sin\nu}{1+e\cos\nu}\left(\theta'+1\right) + 2\left(\theta'+1\right)\frac{L'}{L} + \frac{3\cos\theta\sin\theta}{1+e\cos\nu} = -\frac{c}{1+e\cos\nu}, \tag{13}$$

$$L'' - \frac{2e\sin\nu}{1+e\cos\nu}L' - L\left[\left(\theta'+1\right)^2 - \frac{3\cos^2\theta-1}{1+e\cos\nu}\right] = 0, \tag{14}$$

where $c = \dfrac{I\left(m_2-m_1\right)}{2\left(m_1+m_2+m_t\right)}\dfrac{\mu_m}{\mu\mu_e}\cos i$.

To obtain a deeper understanding of the system's nonlinear dynamics, the in-plane pitch motion during the station-keeping phase is first examined, wherein Equation (13) yields

$$\theta'' - \frac{2e\sin\nu}{1+e\cos\nu}\left(\theta'+1\right) + \frac{3\cos\theta\sin\theta}{1+e\cos\nu} = -\frac{c}{1+e\cos\nu}, \tag{15}$$

Equation (15) is a nonlinear and non-autonomous differential equation describing the in plane motion of tethered satellite system orbits Earth in an inclined elliptical orbit under the influence of Lorenz force. It is evident that as e increases, the damping force weakens, the restoring force becomes less effective, and the external force becomes more pronounced at certain phases of ν. This combination of effects leads to a system that is increasingly sensitive to initial condi-

tions, which can trigger sudden shifts in its dynamics. Consequently, small variations in e or ν can result in large, unpredictable changes in the system's behavior, marking the transition from periodic motion to a chaotic motion.

3. Melnikov Analysis

For small e and c, we introduce a dimensionless small parameter ε ($0<\varepsilon\ll 1$) such that $e=\varepsilon e_1$ and $c=\varepsilon c_1$. After omitting the terms higher than the second order of ε, Equation (15) under small perturbations becomes an integrable Hamiltonian system [28]

$$\theta''+3\sin\theta\cos\theta=\varepsilon\left[2e_1\sin\nu\left(1+\theta'\right)+3e_1\cos\nu\sin\theta\cos\theta-c_1\right]. \tag{16}$$

If $\varepsilon=0$ Equation (16) reduces to the unperturbed planar Hamiltonian system on the form,

$$\theta''+3\sin\theta\cos\theta=0, \tag{17}$$

with first integral of motion gives

$$\frac{1}{2}\theta'^2+\frac{3}{2}\sin^2\theta=E, \tag{18}$$

where E is a constant that denotes the total energy of the system. The phase plane of the unperturbed system is depicted in **Figure 2**, contains two hyperbolic saddle points, $p_i=\left(\mp\pi/2,0\right)$, $i=1,2$. The unstable and stable manifolds of these points together form heteroclinic orbits, as illustrated in **Figure 3**. The heteroclinic orbits are

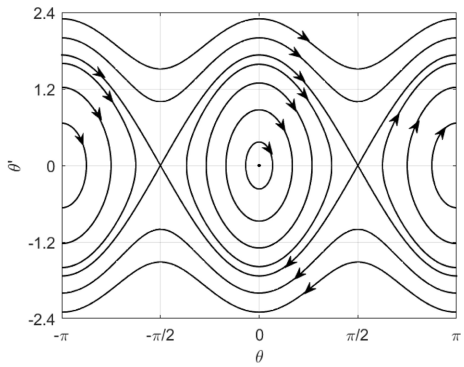

Figure 2. Phase portrait.

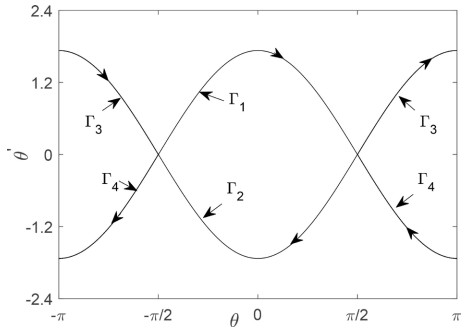

Figure 3. Heteroclinic orbits.

$$\left(\theta_0^{\pm}(v),\theta_0^{\pm'}(v)\right)=\left(\pm\arcsin\left(\tanh\left(\sqrt{3}v\right)\right),\pm\sqrt{3}\,\mathrm{sech}\left(\sqrt{3}v\right)\right). \tag{19}$$

For $\varepsilon\neq 0$, Equation (16) can be written in the form

$$x'=f(x)+\varepsilon g(x,v), \tag{20}$$

where

$$x=\begin{pmatrix}\theta\\ \theta'\end{pmatrix},\ f(x)=\begin{pmatrix}\theta'\\ -\frac{3}{2}\sin 2\theta\end{pmatrix},$$

$$g(x,v)=\begin{pmatrix}0\\ 2e_1\sin v(1+\theta')+e_1\frac{3}{2}\cos v\sin 2\theta-c_1\end{pmatrix}.$$

The perturbation vector $g(x,v)=g(x,v+p)$ is of period $p=2\pi$. After introducing the perturbation term $g(x,v)$, the heteroclinic orbits may divide into stable and unstable manifolds. If these manifolds intersect transversally near the heteroclinic points p_1 and p_2, the perturbed Equation (16) will generate an invariant set where chaos is likely to occur, as described by the Smale horseshoe theory. According to the Melnikov method, when a stable manifold and an unstable manifold intersect, the Melnikov function must have simple zeros. Melnikov function is

$$M_{\pm}(v_0)=\int_{-\infty}^{+\infty} f\left(x_0^{\pm}\right)\wedge g\left(x_0^{\pm},v+v_0\right)\mathrm{d}v,$$

where $\wedge$ denotes the wedge product, which is a standard operation used to compute the determinant formed by two vectors, yields

$$M_{\pm}(v_0)=\int_{-\infty}^{+\infty}\left[2e_1\sin(v+v_0)\left(1+\theta_0^{\pm'}(v)\right)+e_1\frac{3}{2}\cos(v+v_0)\sin 2\theta_0^{\pm}(v)-c_1\right]\theta_0^{\pm'}(v)\mathrm{d}v. \tag{21}$$

Notice that the integral of an odd function over a symmetrical interval is zero. Equation (21) can be simplified to

$$M_{\pm}(v_0)=2e_1I_1\sin v_0+2e_1I_2\sin v_0-e_1\frac{3}{2}I_3\sin v_0-c_1I_4, \tag{22}$$

where

$$\begin{aligned}
I_1&=\int_{-\infty}^{+\infty}\cos v\,\theta_0^{\pm'}(v)\mathrm{d}v,\\
I_2&=\int_{-\infty}^{+\infty}\cos v\,\theta_0^{\pm'2}(v)\mathrm{d}v,\\
I_3&=\int_{-\infty}^{+\infty}\sin v\sin 2\theta_0^{\pm}(v)\,\theta_0^{\pm'}(v)\mathrm{d}v,\\
I_4&=\int_{-\infty}^{+\infty}\theta_0^{\pm'}(v)\mathrm{d}v.
\end{aligned} \tag{23}$$

After calculating integrals, Equation (23) gives

$$I_1=\pm\pi\,\mathrm{sech}\frac{\pi}{2\sqrt{3}},$$

$$I_2=\pi\,\mathrm{csch}\frac{\pi}{2\sqrt{3}},$$

$$I_3 = \pi \operatorname{csch}\frac{\pi}{2\sqrt{3}},$$
$$I_4 = \pm\pi. \tag{24}$$

Therefore, Equation (22) becomes

$$M_{\pm}(v_0) = \pi e_1\left(\pm 2\operatorname{sech}\frac{\pi}{2\sqrt{3}} + \frac{1}{2}\operatorname{csch}\frac{\pi}{2\sqrt{3}}\right)\sin v_0 \mp \pi c_1.$$

If both $M_+(v_0)$ and $M_-(v_0)$ have simple zeros, then there exists a transverse heteroclinic point in the Poincare' map. Notice $|\sin v_0| < 1$, thus, the transverse heteroclinic point exists if,

$$e > \frac{|c|}{\left|\pm 2\operatorname{sech}\frac{\pi}{2\sqrt{3}} + \frac{1}{2}\operatorname{csch}\frac{\pi}{2\sqrt{3}}\right|}, \tag{25}$$

Equation (25) establishes the necessary condition under which chaotic behavior may emerge within this system. From it, we can draw the following cases:

1) At e and $|c|$ equal zero, this case refers to a tethered satellite system orbiting Earth in a circular orbit, with no current flowing through the tether, representing an unperturbed system. The dynamics of this system are illustrated in **Figure 2**.

2) At $e \neq 0$ and $|c| = 0$, this case involves a tethered satellite system orbiting Earth in an elliptical orbit, with no current flowing through the tether. According to Equation (25), the system exhibits chaotic motion as described numerically by Misra [23].

3) At $e = 0$ and $|c| \neq 0$, in this case, the tethered satellite system orbits Earth in a circular orbit with current flowing through the tether. Chaos does not arise because Equation (25) is not satisfied.

4) At $e \neq 0$ and $|c| \neq 0$, in this case, where the tethered satellite system orbits Earth in an elliptical orbit with current flowing through the tether, chaos can be estimated using Equation (25).

4. Tether Length Control

In this section, sliding mode control is used to achieve the chaos control mentioned above by tether length.

By defining the state vector as $\boldsymbol{\theta} = (\theta_1, \theta_2)^{\mathrm{T}} = (\theta, \theta')^{\mathrm{T}}$, Equation (13) can be rewritten in the state-space form

$$\theta_1' = \theta_2$$
$$\theta_2' = \frac{2e\sin v}{1+e\cos v}(\theta_2 + 1) - 2(\theta_2 + 1)u - \frac{3\cos\theta_1 \sin\theta_1}{1+e\cos v} - \frac{c}{1+e\cos v}, \tag{26}$$

where $u = L'/L$ is the control input that can be manipulated using a reel motor on the mother satellite.

The sliding mode surface of the controlled system is defined as:

$$s = \boldsymbol{A}\boldsymbol{e}_{err}^{\mathrm{T}} \tag{27}$$

where $\boldsymbol{A} = [a_1, a_2]$ is a constant vector with $a_2 = 1$ and $a_1 > 0$, (Hurwitz con-

dition).

The state vector of tracking error is

$$\boldsymbol{e}_{err}^{\mathrm{T}} = \begin{bmatrix} e_{err} \\ e'_{err} \end{bmatrix} = \begin{bmatrix} e_2 \\ e_3 \end{bmatrix} = \begin{bmatrix} \theta_1 - \theta_{1d} \\ \theta_2 - \theta_{2d} \end{bmatrix} \tag{28}$$

where $(\theta_{1d}, \theta_{2d})$ are the desired states.

To design the controller, u, the derivative of the sliding mode surface is calculated as follows

$$\begin{aligned} s' &= a_1 e'_2 + e'_3 \\ &= a_1 (\theta'_1 - \theta'_{1d}) + (\theta'_2 - \theta'_{2d}) \\ &= a_1 (\theta'_1 - \theta'_{1d}) + F(\theta, v) - 2(\theta_2 + 1)u - \theta'_{2d}, \end{aligned} \tag{29}$$

where

$$F(\boldsymbol{\theta}, v) = \frac{2e \sin v}{1 + e \cos v}(\theta_2 + 1) - \frac{3 \cos \theta_1 \sin \theta_1}{1 + e \cos v} - \frac{c}{1 + e \cos v}.$$

According to the constant rate reaching law, $s' = -k \operatorname{sign}(s)$, $k > 0$, substituting in Equation (29) yields

$$u = \frac{1}{2(\theta_2 + 1)} \left[a_1 (\theta'_1 - \theta'_{1d}) + F(\theta, v) - \theta'_{2d} + k \operatorname{sign}(s) \right]. \tag{30}$$

According to [29], if k is too small, the reaching time becomes excessively long, which may degrade the controller's performance. Conversely, a large k may lead to chattering, which is undesirable in practical applications.

To ensure the stability of the controlled system, the positive definite Lyapunov function $V = \frac{1}{2} s^2$ is chosen. It follows that

$$V' = ss' = s(-k \operatorname{sign}(s)) = -k|s| < 0. \tag{31}$$

One can see from Equation (31) that the Lyapunov function is negative definite; therefore the controlled system in Equation (26) is asymptotically stable.

5. Numerical Results

Equation (25) indicates that, for small values of eccentricity e and the parameter c, chaos may occur in the dynamical system if this necessary condition is satisfied. From a different perspective, there exists a threshold value below which this condition is not satisfied, and consequently, the system exhibits non-chaotic motion. Tong and Rimrott, in their study of tethered satellites in elliptical orbits established a necessary condition for chaos as $e > 0$, [20]. From these findings, we conclude that the presence of the Lorentz force in the system enables satellites to orbit in a more elliptical orbit without chaotic behavior and the need for active control.

To validate this conclusion, numerical simulations are performed. Initially, in **Figure 4**, a bifurcation diagram of e is plotted at $c = 0$, where the vertical axis variable θ has been defined as the sampled values of the solution θ over a fixed range of the true anomaly v, to explicitly identify the threshold eccentricity value at which chaos emerges. Subsequently, in **Figure 5**, a bifurcation diagram of

c at $e=0$, is presented to illustrate the impact of varying c on system dynamics and to define critical ranges of this parameter. Finally, Figure 6 presents a bifurcation diagram of e at $|c|=0.25\times10^{-3}$, demonstrated that increasing eccentricity is possible while maintaining periodic motion due to the stabilizing influence of the Lorentz force. This observation is further clarified by Figure 7, which shows a Poincaré section at $c=0$ and $e=0.6\times10^{-4}$, clearly indicating chaotic motion, as further clarified by Figure 8. However, when the parameter c is altered to -0.25×10^{-3}, the system exhibits periodic motion, as depicted in Figure 9 and Figure 10. It should be noted that the Melnikov analysis, which produced the necessary condition described by Equation (25), relies on the assumption of small values for both parameters e and c.

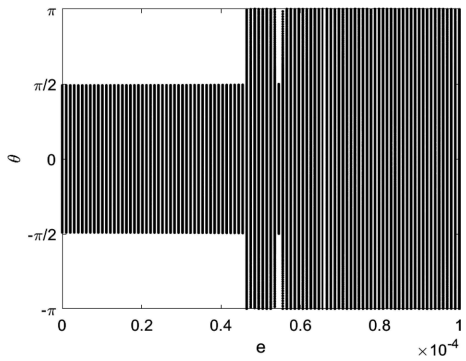

Figure 4. Bifurcation diagram of e at $c=0$.

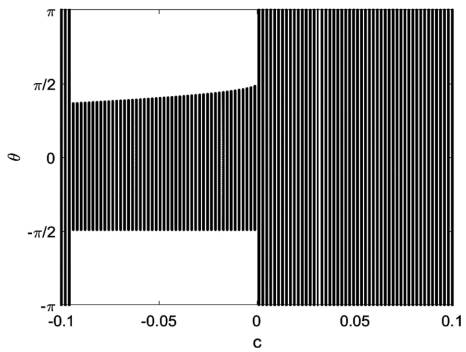

Figure 5. Bifurcation diagram of c at $e=0$.

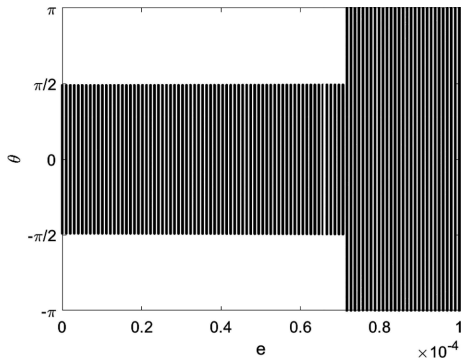

Figure 6. Bifurcation diagram of e at $|c|=0.25\times10^{-3}$.

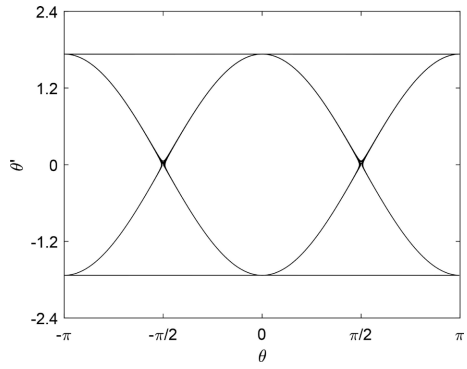

Figure 7. Poincaré section at $c = 0$ and $e = 0.6 \times 10^{-4}$.

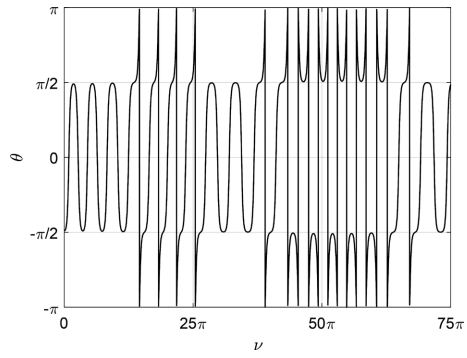

Figure 8. Pitch angle versus ν at $c = 0$ and $e = 0.6 \times 10^{-4}$.

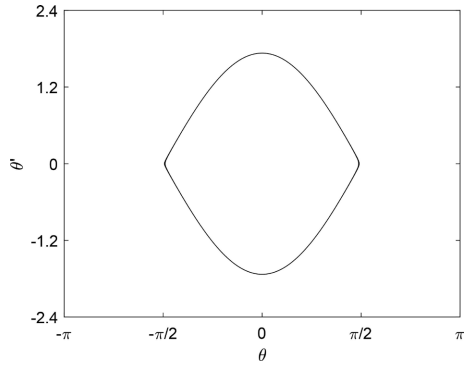

Figure 9. Poincaré section at $c = -0.25 \times 10^{-3}$ and $e = 0.6 \times 10^{-4}$.

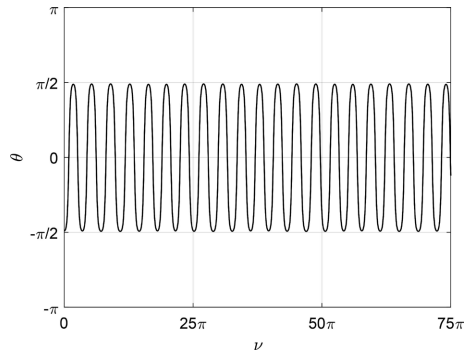

Figure 10. Pitch angle versus ν at $c = -0.25 \times 10^{-3}$ and $e = 0.6 \times 10^{-4}$.

To demonstrate the chaotic behavior and its control, the TiPS (Tether Physics and Survivability Experiment) mission is modelled. The TSS operated in a near-circular orbit. Its primary focus was to analyze how the tether interacted with Earth's magnetic field and ionosphere. The mission was a success, demonstrating stable tether behaviour and offering critical insights for the development of future electrodynamic propulsion systems. Our study expands on the mission by exploring the dynamics of the system in elliptical orbits, providing a broader understanding of tether performance under varied orbital conditions. The system consisted of a mother satellite with a mass of approximately 1020 kg, connected to a subsatellite with a mass of 70 kg. The two satellites were linked by a tether with a length of 4 km and a mass of about 3.4 kg. The system operated at an altitude of approximately 600 km, with an orbital inclination of 63˚.

To gain a deeper insight into the chaotic motion of the electrodynamic tethered satellite system in an inclined plane, we select $e=0.6\times10^{-3}$ and $I=1\,\text{mA}$, which lie within the chaotic zone depending on Equation (25). Additionally, the system is initialized with the states $(\theta,\theta')=(-\pi/2+\pi/100,0)$, where $\pi/100$ is a given perturbed angle, positioning the system near one of the unstable saddle points $(\mp\pi/2,0)$. Figure 11 illustrates that the pitch motion exhibits characteristics of an irregular oscillator. Figure 12 presents the phase plane of the perturbed system, with dots representing the Poincaré section. It indicates that the system exhibits chaotic behavior. To provide further clarification, we focus on the saddle point in Figure 13.

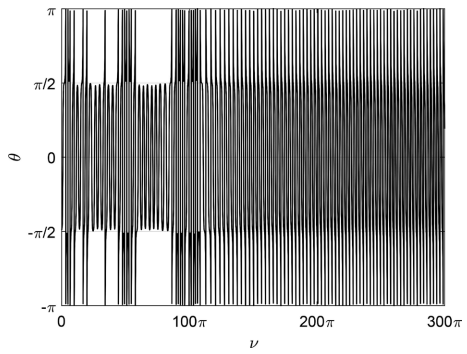

Figure 11. Pitch angle versus ν $e=0.6\times10^{-3}$ and $I=1$ mA.

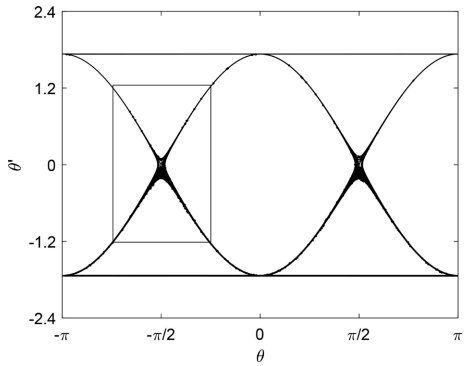

Figure 12. Poincaré section at $e=0.6\times10^{-3}$ and $I=1$ mA.

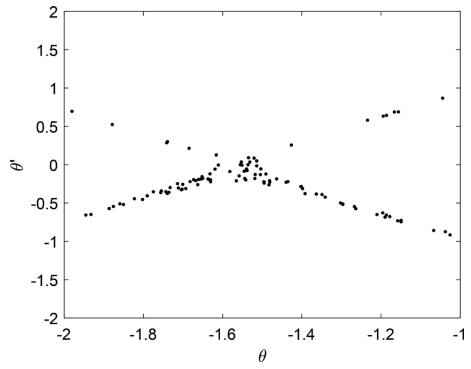

Figure 13. Zoom in on saddle point.

In the absence of electromagnetic forces in circular orbit, for the unperturbed motion, **Figure 14** demonstrates that the pitch angle undergoes periodic oscillations with a period of 11.2155. **Figure 15** presents the Poincaré section, which shows that the Poincaré points converge to a single point, indicating that the motion is periodic. This result demonstrates that the chaotic motion arises as a result of the combined effects of the elliptical orbit and electromagnetic forces.

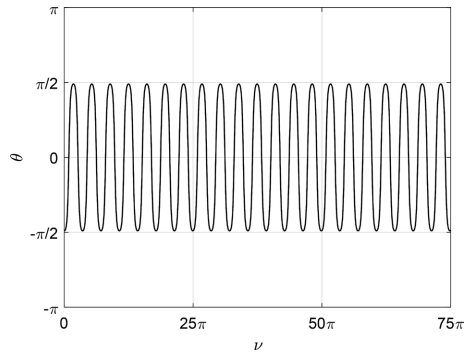

Figure 14. Pitch angle versus ν for the unperturbed system.

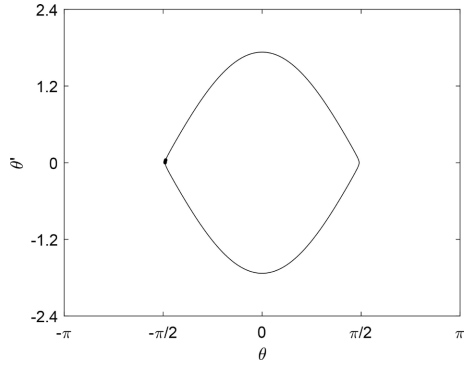

Figure 15. Poincaré section for the unperturbed system.

Furthermore, an additional case is conducted to verify the validity of the chaotic zone, in which the orbital eccentricity is altered to 0.6×10^{-4}, and current to be 10 mA, in this case, Equation (25) is not satisfied, meaning the parameters fall outside

the chaotic zone. Figure 16 and Figure 17 demonstrate that the system exhibits periodic motion with a period of 10.6814.

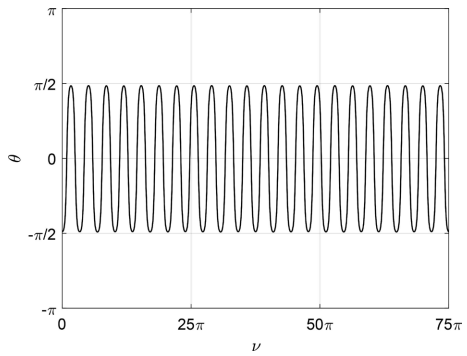

Figure 16. Pitch angle versus ν at $e = 0.6 \times 10^{-4}$ and $I = 10$ mA.

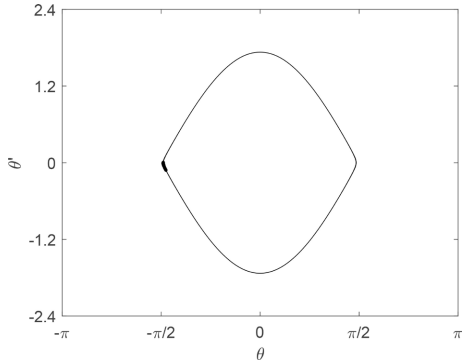

Figure 17. Poincaré section at $e = 0.6 \times 10^{-4}$ and $I = 10$ mA.

In the following, the effectiveness of tether length control using a sliding mode controller is evaluated. This controller can be utilized to suppress the chaotic motion presented in Figure 11 and Figure 12, allowing the system to achieve either a desired oscillatory behavior or even steer a chaotic motion toward a predefined pitch angle through the proposed control law.

Figure 18 and Figure 19 indicate the controller's capability to stabilize the system into a desired oscillatory state. As shown, the controlled system exhibits periodic behavior, as the unperturbed system, with a period of 11.2155.

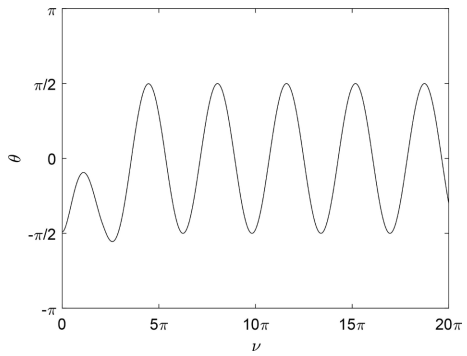

Figure 18. Pitch angle versus ν for the controlled system achieving periodic motion.

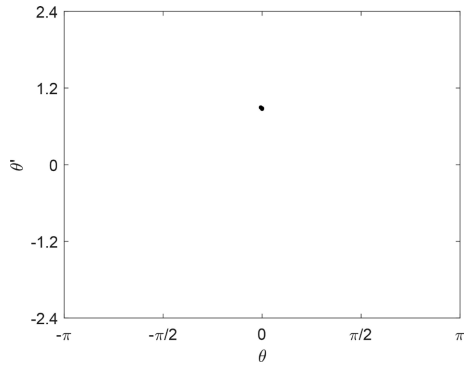

Figure 19. Poincaré section for the controlled system achieving periodic motion.

Figure 20 and **Figure 21** demonstrate that the controller successfully guides chaotic motion toward the desired equilibrium point $(-\pi/2,0)$, starting from the initial condition $(-\pi/3,0)$. **Figure 20** depicts the pitch angle as a function of the true anomaly, ν, clearly illustrating convergence toward the desired equilibrium. Furthermore, the Poincaré section, **Figure 21**, clearly illustrates convergence toward the desired equilibrium point $(-\pi/2,0)$.

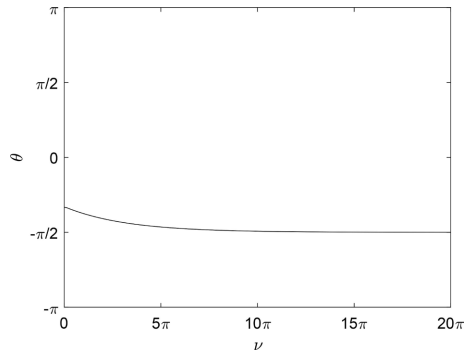

Figure 20. Pitch angle versus ν for the controlled system reaching the desired point.

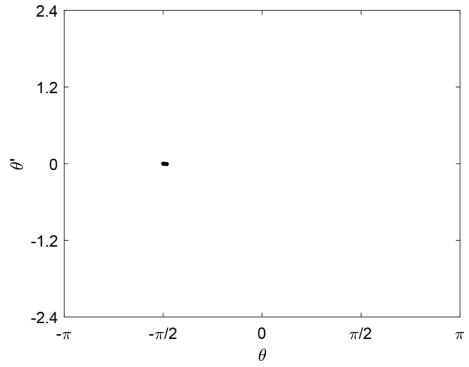

Figure 21. Poincaré section for the controlled system reaching the desired point.

6. Conclusion

The tethered satellite system is modelled as two masses connected by a tether, orbiting Earth in an inclined elliptical orbit and influenced by the Lorentz force re-

sulting from the current flowing through the tether and Earth's magnetic field. The attitude equations are derived using the Lagrangian method. Chaos is demonstrated through transversal heteroclinic orbits, and the parameter domain for chaos occurrence is identified using the necessary condition resulting from the Melnikov function. This indicates that for small values of eccentricity and the parameter representing the Lorenz force, an electrodynamic tethered satellite system can achieve a more elliptical orbit around the Earth than a traditional tethered satellite system without exhibiting chaotic behavior. The sliding mode control strategy can effectively regulate the chaotic motion, guiding it toward a desired trajectory through controlled deployment and retrieval of the tether. This study is limited to theoretical modeling and numerical simulations; future work should include experimental validation and high-fidelity simulations to assess the control strategy's practical feasibility. Investigating tether flexibility and alternative control methods may also advance research in this field.

Conflicts of Interest

The authors declare no conflicts of interest regarding the publication of this paper.

References

[1] Huang, P., Zhang, F., Chen, L., Meng, Z., Zhang, Y., Liu, Z., *et al.* (2018) A Review of Space Tether in New Applications. *Nonlinear Dynamics*, **94**, 1-19. https://doi.org/10.1007/s11071-018-4389-5

[2] Kumar, K.D. (2006) Review on Dynamics and Control of Nonelectrodynamic Tethered Satellite Systems. *Journal of Spacecraft and Rockets*, **43**, 705-720. https://doi.org/10.2514/1.5479

[3] Modi, V., Lakshmanan, P. and Misra, A. (1990) Dynamics and Control of Tethered Spacecraft—A Brief Overview. *Dynamics Specialists Conference*, Long Beach, 5-6 April 1990, 1195. https://doi.org/10.2514/6.1990-1195

[4] Sanmartin, J.R., Lorenzini, E.C. and Martinez-Sanchez, M. (2010) Electrodynamic Tether Applications and Constraints. *Journal of Spacecraft and Rockets*, **47**, 442-456. https://doi.org/10.2514/1.45352

[5] Jang, W., Yoon, Y., Go, M. and Chung, J. (2025) Dynamic Behavior and Libration Control of an Electrodynamic Tether System for Space Debris Capture. *Applied Sciences*, **15**, Article No. 1844. https://doi.org/10.3390/app15041844

[6] Sánchez-Arriaga, G., Lorenzini, E.C. and Bilén, S.G. (2024) A Review of Electrodynamic Tether Missions: Historical Trend, Dimensionless Parameters, and Opportunities Opening Space Markets. *Acta Astronautica*, **225**, 158-168. https://doi.org/10.1016/j.actaastro.2024.09.002

[7] Gao, F., Li, J., Dong, F., Ji, Y. and Sun, G. (2024) Dynamic Modeling and Control Strategy for Tethered Satellite Systems in Orbital Debris Management. *Acta Mechanica Sinica*, **41**, Article ID: 524262. https://doi.org/10.1007/s10409-024-24262-x

[8] Mróz, P., Otarola, A., Prince, T.A., Dekany, R., Duev, D.A., Graham, M.J., *et al.* (2022) Impact of the Spacex Starlink Satellites on the Zwicky Transient Facility Survey Observations. *The Astrophysical Journal Letters*, **924**, L30. https://doi.org/10.3847/2041-8213/ac470a

[9] Tao, H., Che, X., Zhu, Q. and Li, X. (2022) Satellite In-Orbit Secondary Collision Risk

Assessment. *International Journal of Aerospace Engineering*, **2022**, Article ID: 6358188. https://doi.org/10.1155/2022/6358188

[10] Ledkov, A. and Aslanov, V. (2022) Review of Contact and Contactless Active Space Debris Removal Approaches. *Progress in Aerospace Sciences*, **134**, Article ID: 100858. https://doi.org/10.1016/j.paerosci.2022.100858

[11] Svotina, V.V. and Cherkasova, M.V. (2023) Space Debris Removal—Review of Technologies and Techniques. Flexible or Virtual Connection between Space Debris and Service Spacecraft. *Acta Astronautica*, **204**, 840-853. https://doi.org/10.1016/j.actaastro.2022.09.027

[12] Ledkov, A. and Aslanov, V. (2019) Evolution of Space Tethered System's Orbit during Space Debris Towing Taking into Account the Atmosphere Influence. *Nonlinear Dynamics*, **96**, 2211-2223. https://doi.org/10.1007/s11071-019-04918-6

[13] Lim, J. and Chung, J. (2018) Dynamic Analysis of a Tethered Satellite System for Space Debris Capture. *Nonlinear Dynamics*, **94**, 2391-2408. https://doi.org/10.1007/s11071-018-4498-1

[14] Huang, W., He, D., Li, Y., Zhang, D., Zou, H., Liu, H., *et al.* (2022) Nonlinear Dynamic Modeling of a Tether-Net System for Space Debris Capture. *Nonlinear Dynamics*, **110**, 2297-2315. https://doi.org/10.1007/s11071-022-07718-7

[15] Li, X., Yang, K. and Zhang, J. (2024) The Dynamic Instability Analysis of Electrodynamic Tether System. *Nonlinear Dynamics*, **112**, 13771-13784. https://doi.org/10.1007/s11071-024-09771-w

[16] Xie, M., Lu, H., Wang, C., Li, A. and Zabolotnov, Y. (2025) Analysis and Control of the Equilibrium Position in Bare Electrodynamic Tether Systems. *Acta Astronautica*, **226**, 60-70. https://doi.org/10.1016/j.actaastro.2024.11.006

[17] Ahn, Y., Jang, W., Lee, J. and Chung, J. (2024) Dynamic Analysis of Tethered Satellites with a Payload Moving along a Flexible Tether. *Applied Sciences*, **14**, Article No. 9498. https://doi.org/10.3390/app14209498

[18] Yu, B.S., Xu, S.D. and Jin, D.P. (2020) Chaos in a Tethered Satellite System Induced by Atmospheric Drag and Earth's Oblateness. *Nonlinear Dynamics*, **101**, 1233-1244. https://doi.org/10.1007/s11071-020-05844-8

[19] Salazar, F.J.T. and Prado, A.F.B.A. (2022) Suppression of Chaotic Motion of Tethered Satellite Systems Using Tether Length Control. *Journal of Guidance, Control, and Dynamics*, **45**, 580-586. https://doi.org/10.2514/1.g006364

[20] Tong, X. and Rimrott, F.P.J. (1991) Numerical Studies on Chaotic Planar Motion of Satellites in an Elliptic Orbit. *Chaos, Solitons & Fractals*, **1**, 179-186. https://doi.org/10.1016/0960-0779(91)90007-v

[21] Karasopoulos, H. and Richardson, D. (1992). Chaos in the Pitch Equation of Motion for the Gravity-Gradient Satellite. *Guidance, Navigation and Control Conference*, Hilton Head Island, 10-12 August 1992, 4369. https://doi.org/10.2514/6.1992-4369

[22] Fujii, H.A. and Ichiki, W. (1997) Nonlinear Dynamics of the Tethered Subsatellite System in the Station Keeping Phase. *Journal of Guidance, Control, and Dynamics*, **20**, 403-406. https://doi.org/10.2514/2.4057

[23] Misra, A.K., Nixon, M.S. and Modi, V.J. (2001) Nonlinear Dynamics of Two-Body Tethered Satellite Systems: Constant Length Case. *The Journal of the Astronautical Sciences*, **49**, 219-236. https://doi.org/10.1007/bf03546319

[24] Pelaez, J. and Lara, M. (2003) Periodic Solutions in Electrodynamic Tethers on Inclined Orbits. *Journal of Guidance, Control, and Dynamics*, **26**, 395-406. https://doi.org/10.2514/2.5077

[25] Kojima, H. and Sugimoto, T. (2009) Stability Analysis of In-Plane and Out-of-Plane Periodic Motions of Electrodynamic Tether System in Inclined Elliptic Orbit. *Acta Astronautica*, **65**, 477-488. https://doi.org/10.1016/j.actaastro.2009.02.006

[26] Aslanov, V. and Ledkov, A. (2012) Dynamics of Tethered Satellite Systems. Elsevier.

[27] Stevens, R.E. (2008) Optimal Control of Electrodynamic Tether Satellites. Ph.D. Thesis, Air Force Institute of Technology.

[28] Liu, Y. and Chen, L. (2013) Chaos in Attitude Dynamics of Spacecraft. Springer.

[29] Liu, J. (2017) Sliding Mode Control Using Matlab. Academic Press.